Coronal mass ejections and space weather

D. F. Webb[1] and N. Gopalswamy[2]

[1] Institute for Scientific Research, Boston College, 140 Commonwealth Ave., Chestnut Hill, MA 02467 USA
[2] NASA Goddard Space Flight Center, Code 695.0, Greenbelt, MD 20771, USA

Abstract. Coronal mass ejections (CMEs) are a key feature of coronal and interplanetary (IP) dynamics. Major CMEs inject large amounts of mass and magnetic fields into the heliosphere and, when aimed Earthward, can cause major geomagnetic storms and drive IP shocks, a key source of solar energetic particles. Studies over this solar cycle using the excellent data sets from the SOHO, TRACE, Yohkoh, Wind, ACE and other spacecraft and ground-based instruments have improved our knowledge of the origins and early development of CMEs at the Sun and how they affect space weather at Earth. A new heliospheric experiment, the Solar Mass Ejection Imager, has completed 3 years in orbit and has obtained results on the propagation of CMEs through the inner heliosphere and their geoeffectiveness. We review key coronal properties of CMEs, their source regions, their manifestations in the solar wind, and their geoeffectiveness. Halo-like CMEs are of special interest for space weather because they suggest the launch of a geoeffective disturbance toward Earth. However, not all halo CMEs are equally geoeffective and this relationship varies over the solar cycle. Although CMEs are involved with the largest storms at all phases of the cycle, recurrent features such as interaction regions and high speed wind streams can also be geoeffective.

Index Terms. Coronal mass ejection, magnetic field reconnection, solar wind plasma, solar-terrestrial relations.

---

1. Introduction: solar and geomagnetic activity over the solar cycle

The level of geomagnetic activity tends to follow the solar sunspot cycle. The overall correspondence between the sunspot and geoactivity cycles can be seen in long-term plots comparing indices of the two kinds of activity. On an annual basis, the geoactivity cycle has more structure than the solar cycle. Fig. 1 shows that the geomagnetic index *Ap* is more variable than sunspot number, but does tend to track the sunspot cycles in amplitude. The figure also illustrates the double-peaked nature of the geoactivity cycle, with a peak near sunspot maximum and another often higher peak during the declining phase. These peaks vary in amplitude and timing, and the peak around maximum may be multiple. The two main peaks represent the maximum phases of two components of geoactivity with different solar and heliospheric sources: the first associated with transient solar activity, i.e., CMEs, that tracks the solar cycle in amplitude and phase, and the later peak with recurrent high speed streams from coronal holes.

Richardson et al. (2002) studied the relative contributions of different types of solar wind structures to the *aa* index from 1972-2000. They identified CME-related flows, corotating high-speed streams, and slow flows near the Earth, finding that each type contributed significantly to *aa* at all phases of the cycle. For example, CMEs contribute ~50% of *aa* at solar maximum and ~10% at minimum, whereas high speed streams contribute ~70% at minimum and ~30% at maximum. Thus, both types of sources, CMEs and coronal holes/high speed streams, contribute to geoactivity during all phases of the cycle. CMEs, however, are responsible for the most geoeffective solar wind disturbances and, therefore, the largest storms.

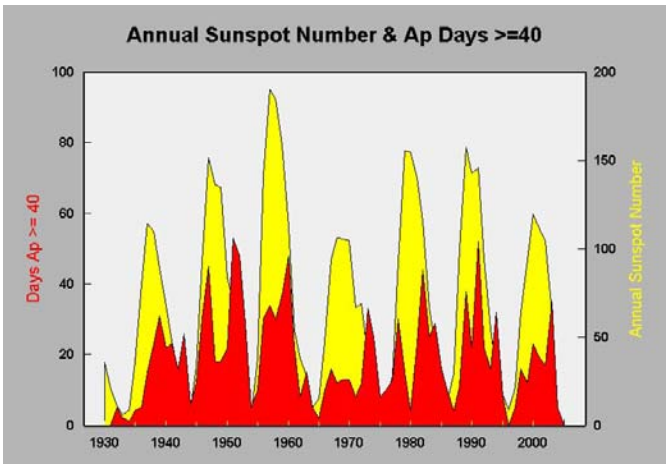

Fig. 1. Annual number of geomagnetic disturbed days with Ap index > 40 (black area) vs. annual sunspot number (light area) for solar cycles 17-23. Courtesy NOAA Geophysical Data Center, Boulder, CO, USA.

CMEs consist of large structures containing plasma and magnetic fields that are expelled from the Sun into the heliosphere. The plasma observed in a CME is entrained on

expanding magnetic field lines, which can have the form of helical field lines with changing pitch angles, such as a flux rope. In this paper we review the best-determined coronal properties of CMEs including what we know about their source regions near the surface, and some key signatures of CMEs in the solar wind. We emphasize observations of halo CMEs, as observed by the SOHO LASCO coronagraphs, because they are important for space weather studies.

2. Properties of CMEs

Most observations of CMEs have been made in space by coronagraphs, viewing structures in white light via the Thomson-scattering process. The LASCO coronagraphs (Brueckner et al., 1995) provide the most recent and most extensive spaceborne white light observations of CMEs. These data have been acquired since early 1996, providing fairly continuous coverage of the corona and CMEs over most of cycle 23 from solar activity minimum through its current declining phase. The LASCO CME observations are complemented by other SOHO instruments at coronal wavelengths, especially EIT, UVCS and CDS, and the Yohkoh and TRACE spacecraft (see Hudson & Cliver, 2001).

The measured properties of CMEs include their occurrence rates, locations relative to the solar disk, angular widths, speeds, masses and energies (see Kahler, 1992; St. Cyr et al., 2000; Webb, 2002; Yashiro et al., 2004; Gopalswamy et al., 2005; Gopalswamy, 2006; Kahler, 2006). There is a large range in the basic properties of CMEs, although some of this scatter is due to projection effects (Burkepile et al., 2004). Their speeds, accelerations, masses and energies extend over 2-3 orders of magnitude (see Vourlidas et al., 2002; Gopalswamy, 2006), and their angular widths exceed, by factors of 3 to 10 the sizes of flaring active regions. Note that these measured values make the assumption that all the CME material is in the “plane of the sky”, the plane orthogonal to the Sun-Earth line. Thus, for example, unless a CME is exactly at the solar limb, its derived speed will be an underestimate and the width an overestimate.

CMEs can exhibit a variety of forms, some having the classical “three-part” structure and others being more complex with bright interiors. The basic structure of the former kind consists of a bright leading arc followed by a darker, low-density cavity and a bright core of denser material (Fig. 2). Different forms of CMEs have been observed, including those with large circular regions resembling flux ropes and halo CMEs.

Because of their increased sensitivity, field of view and dynamic range, the SOHO LASCO coronagraphs now frequently observe halo CMEs, which appear as expanding, circular brightenings that completely surround the coronagraphs’ occulting disks (Howard et al., 1982). This suggests that these are ‘normal’ CMEs seen in projection (Burkepile et al., 2004) to be moving outward either toward or away from the Earth. Observations of associated activity on the solar disk are necessary to distinguish whether a halo CME was launched from the front or backside of the Sun. CMEs which have a larger apparent angular size (usually > 120^{o}) than typical limb CMEs but do not appear as complete

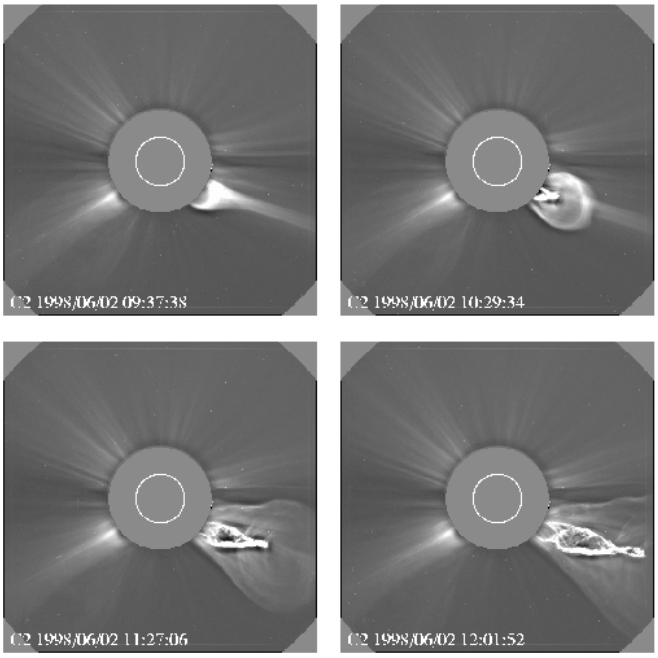

Fig. 2. Evolution of a "3-part" CME observed by the LASCO C2 coronagraph on 2 June 1998. Note the circular structures just above the prominence, suggesting a flux rope. From Plunkett et al. (2000).

halos, are called ‘partial halo’ CMEs. Halo CMEs are important for three reasons: 1) They are the key link between solar eruptions and many space weather phenomena such as major storms and solar energetic particle events; 2) The source regions of frontside halo CMEs are usually located within a few tens of degrees of Sun center, as viewed from Earth (Cane et al., 2000; Webb, 2002; Gopalswamy, 2004). Thus, these regions can be studied in greater detail than for most CMEs, which are observed near the limb; 3) Frontside halo CMEs must travel approximately along the Sun-Earth line, so their internal material can be sampled in situ by spacecraft near the Earth. Three spacecraft, SOHO, Wind and ACE, now provide solar wind measurements upstream of Earth.

The frequency of occurrence of CMEs observed in white light tends to track the solar cycle in both phase and amplitude, which varies by an order of magnitude over the cycle (Webb and Howard, 1994). LASCO has now observed from solar minimum in early 1996 through the declining phase of the current (23^{rd}) solar cycle (Fig. 3). It has detected CMEs at a rate slightly higher than earlier observations, reaching nearly 6/day at maximum (St. Cyr et al., 2000;

Gopalswamy et al., 2005; Gopalswamy 2006). Halo CMEs occur at a rate of about 10% that of all CMEs, but full halo CMEs are only detected at a rate of ~4% of all CMEs. If CMEs occurred randomly at all longitudes and LASCO detected them all, this rate would be about 15%, suggesting that LASCO sees as halos CMEs that are brighter (or denser) than average. In turn this implies that LASCO may miss fainter CMEs near sun center. Supporting this, Tripathi et al. (2004) found that all (8%) post-eruptive EIT arcades not associated with LASCO CMEs occurred within 40º of sun center.

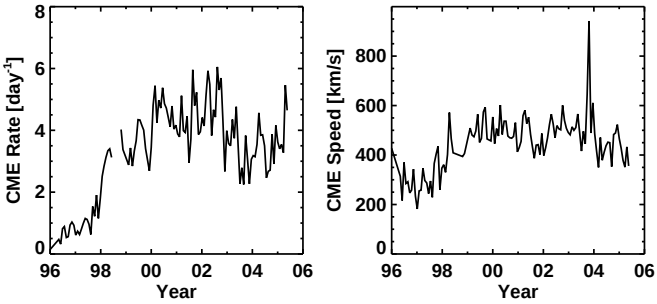

Fig. 3. LASCO CME occurrence rate (left) and mean speed (right) from 1996 into 2005 averaged over Carrington Rotations. The big spike in CME speed is due to CMEs in the Halloween 2003 period. From Gopalswamy (2006).

The latitude distribution of the central position angles of CMEs tends to cluster about the equator at minimum but broadens to cover all latitudes near solar maximum. Hundhausen (1993) noted that this CME latitude variation more closely parallels that of streamers and prominences than of active regions, flares or sunspots. This pattern including the match between CMEs and associated prominence eruptions has been confirmed with the LASCO data (see Fig. 7 in Gopalswamy, 2004).

With the SMM (Hundhausen, 1993) and Solwind (Howard et al., 1985) coronagraphs, the angular size distribution of CMEs seemed to vary little over the cycle, maintaining an average width of about 45º. However, the CME size distribution observed by LASCO is affected by its increased detection of very wide CMEs, especially halos. Including halo CMEs from Jan. 1996-June 1998, St. Cyr et al. (2000) found

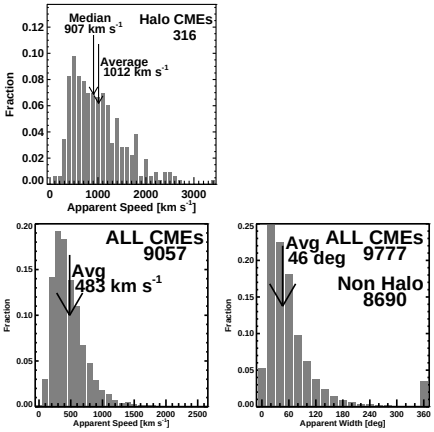

Fig. 4. Histograms of speeds (left) and widths (middle) of all LASCO CMEs and all halo CMEs (right) from 1996 to June 2005. The average of each distribution is marked with an arrow. Note that the average speed of halo CMEs is twice that of all CMEs. From Gopalswamy (2006).

the average (median) width of LASCO CMEs was 72º (50º). Including all measured LASCO CMEs of 20-120º in width through 2002, Yashiro et al. (2004) found that the average widths (Fig. 4) varied from 47º at minimum to 61º just before maximum (1999), then declining again.

Estimates of the apparent speeds of the leading edges of CMEs range from about 20 to >2500 km/s, or from well below the sound speed in the lower corona to well above the Alfven speed (Fig. 4). The annual average speeds of SOLWIND and SMM CMEs varied over the solar cycle from about 150-475 km/s, but their relationship to sunspot number was unclear (Howard et al., 1986; Hundhausen et al., 1994). However, LASCO CME speeds clearly increase with sunspot number in this cycle (St. Cyr et al., 2000; Yashiro et al., 2004; Gopalswamy, 2006), from 280 at solar minimum to 500 km/s near maximum (Fig. 3). The annual average speed of full halo CMEs is ~2 times greater than that of all CMEs (Fig. 4; Webb, 2002; Yashiro et al., 2004), suggesting that LASCO sees as halos CMEs which are usually faster and, hence, more energetic than the average CME. Above a height of about $2R_s$ the speeds of typical CMEs are relatively constant, although the slowest CMEs tend to show acceleration while the fastest decelerate (St. Cyr et al., 2000; Yashiro et al., 2004; Gopalswamy, 2006). The acceleration for most CMEs occurs low in the corona (< $2R_s$).

Finally, the masses and energies of CMEs require difficult instrument calibrations and have large uncertainties. The average mass of CMEs derived from the older coronagraph data (Skylab, SMM and Solwind) was a few times 10^{15} g. LASCO calculations indicate a lower average CME mass, likely because LASCO can measure masses down to 10^{13} g (Vourlidas et al., 2002; Gopalswamy, 2006). Studies, using Helios (Webb et al., 1996) and LASCO (Vourilidas et al., 2000) data, suggest that the older CME masses may also have been underestimated because mass outflow can continue well

after the CME's leading edge leaves the instrument field of view. Recent LASCO results of the mass density of CMEs as a function of height show that this density rises until ~8Rs, then levels off (Howard et al., 2003). This suggests that CMEs with larger masses reach greater heights, and are more likely to escape the Sun. Indeed, there is a population with a mass peak <8Rs; these CMEs are less massive and slower and may not reach IP space. Mass estimates of a few CMEs have also been made with radio (Gopalswamy and Kundu, 1993; Ramesh et al., 2003) and X-ray observations (see Rust and Hildner, 1976; Hudson and Webb, 1997). These estimates are usually lower than that of the equivalent white light masses. The radio and X-ray techniques provide an independent check on CME masses because their dependency is on the thermal properties of the plasma (density and temperature) vs only density in the white light observations. Likewise average CME kinetic energies measured by LASCO are less than previous measurements, $<10^{30}$ erg. The CME kinetic energy distribution has a power law index of -1 (Vourlidas et al., 2002) different than that for flares (-2; Hudson 1991).

3. The solar signatures of CMEs

Next we briefly summarize our knowledge of near-solar surface features that appear associated with the initiation of CMEs (see recent reviews, such as Webb, 2002; Cliver & Hudson, 2002; Gopalswamy, 2004; Kahler, 2006). CMEs in general are associated with previously closed magnetic field regions. Many CMEs viewed at the limb appear to arise from large-scale, preexisting coronal streamers (see Hundhausen, 1993). Many energetic CMEs involve the disruption, or "blowout" of such a structure, which increases in brightness and size for days before erupting as a CME (Howard et al., 1985; Hundhausen, 1993).

Comparisons of low coronal soft X-ray, EUV and radio data with the white light observations provide many insights into the source regions of CMEs. Previous statistical association studies indicated that erupting prominences (EPs) and X-ray events, especially of long duration, were the most common near-surface activity associated with CMEs. Recently, Gopalswamy et al. (2003) showed that 73% of microwave EPs, and nearly all those attaining high heights, were associated with CMEs, confirming results first found during Skylab (see Munro et al., 1979). There is a strong correspondence between X-ray ejecta and CMEs. Nitta and Akiyama (1999) found that flares with X-ray ejecta were always associated with CMEs and the X-ray ejecta corresponded with CME cores, likely dense, heated prominence material (also see Rust and Webb, 1977). Most optical flares occur independently of CMEs and even those accompanying CMEs may be a consequence rather than a cause of the eruption. The fastest, most energetic CMEs, however, are usually also associated with surface flares, and reported flares are associated with most frontside, full halo CMEs (see Webb, 2002). This rate may be high because the sources of halo CMEs can be clearly viewed near sun center, and halo CMEs are faster and more energetic than average CMEs. Thus, either or both mass motion, or ejection, and speed seem to be critical for the association of a flare with a CME.

Sheeley et al. (1983) first showed that the probability of associating a CME with a soft X-ray flare increased linearly with the flare duration, reaching 100% for flare events of duration >6 hours. The SMM CME observations indicated that the estimated departure time of flare-associated CMEs typically preceded the flare onsets. Harrison (1986) found that such CMEs were initiated during weaker soft X-ray bursts that preceded any subsequent main flare by tens of minutes, and that the main flares were often spatially offset to one side of the CME.

The latitude distribution of LASCO CMEs peaks at the equator, but the distribution of EIT EUV activity associated with these CMEs is bimodal with peaks 30º north and south of the equator (Plunkett et al., 2002). This offset is confirmed for the distribution of sources associated with halo CMEs (Fig. 5 - Webb 2002). This pattern indicates that many CMEs can involve more complex, multiple polarity systems (Webb et al., 1997) such as modeled by Antiochos et al. (1999).

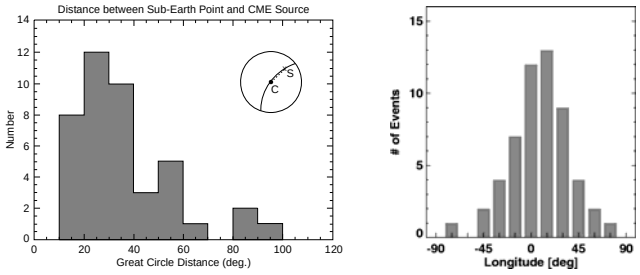

Fig. 5. Histograms of source longitudes of halo CMEs (left - Webb, 2002) and strongly geoeffective CMEs (right - Gopalswamy et al., 2005).

The most obvious coronal signatures of CMEs in the low corona are the arcades of bright loops which develop after the CME material has apparently left the surface (Kahler, 1977-Skylab; Hudson & Webb, 1997-Yohkoh; Tripathi et al., 2004-EIT-Fig. 6). Prior to the eruption, an S-shaped structure called a sigmoid can develop, sometimes in association with filament activation. A sigmoid is indicative of a highly sheared, non-potential coronal magnetic field, and might be an important precursor of a CME (see Canfield et al., 1999), although its geoeffectiveness has not been established. Eventually an eruptive flare can occur, resulting in the bright, long-duration arcade of loops. Sterling et al. (2000) call this process "sigmoid-to-arcade" evolution. These arcades suggest the eruption and subsequent reconnection of strong magnetic field lines associated with the CME system. Tripathi et al. (2004) find that nearly all (92%) EIT post-eruptive arcades from 1997-2002 were associated with

LASCO CMEs. Dimming regions observed in X-rays and in EUV imply that material is evacuated from the low corona (Hudson & Webb, 1997). The dimming regions can be much more extensive than the flaring activity and can map out the apparent base of the white light CME (Thompson et al., 2000). Thus, the dimming events appear to be one of the earliest and best-defined signatures in soft X-ray and EUV emission of the actual mass ejected from the low corona.

Surveys of solar activity associated with frontside halo CMEs have been made primarily with low coronal images from the EIT and Yohkoh SXT instruments. The activity associated with halo CMEs includes the formation of dimming regions, long-lived loop arcades, flaring active regions, large-scale coronal waves, and filament eruptions. Specifically, Webb (2002) finds that 2/3 of halo CMEs were associated with either or both filament eruptions and dimmings. The frequent detection of coronal EUV waves was an exciting discovery of the EIT observations. Although Biesecker et al. (2002) found a CME associated with nearly every EIT wave, apparently not all CMEs are associated with waves. For example, Webb (2002) found that only about half of frontside halo CMEs have EIT waves, and Cliver et al. (2005) that there are ~5 times as many frontside CMEs as EIT waves.

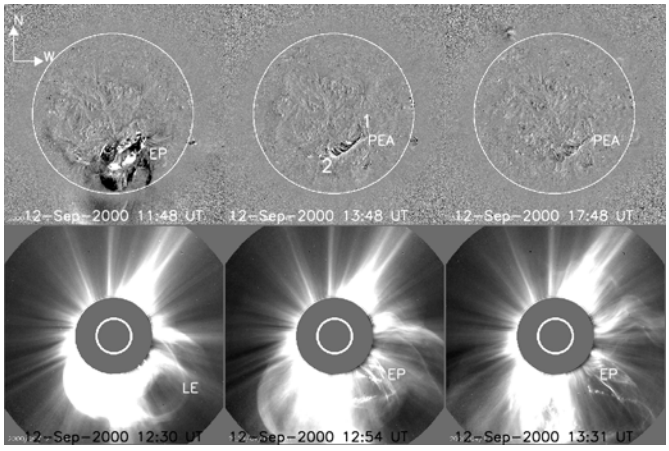

Fig. 6. Erupting prominence, dimming regions & arcade associated with a fast CME on 12 Sept. 2000. Top: EIT 195A running-difference images; bottom: CME leading edge and EP seen in LASCO C2 images. From Tripathi et al. (2004).

Type II and IV radio bursts are associated with CMEs. Type IV bursts, especially "moving", imply magnetic plasma ejections, possibly associated with EPs, and nonthermal particles from field-line reconnection. SOHO data now seem to confirm that type II bursts arise from shock waves driven by CMEs (Cliver et al., 1999; Gopalswamy et al., 2005). Type II bursts in various wavelength domains appear to be organized by the kinetic energy of the CMEs: metric type II bursts (<2 Rs) are associated with CMEs with above-average kinetic energy; those extending into decameter-hectometric (DH) wavelengths (>2 Rs) have moderate CME kinetic energy; and type II bursts seen in both the metric and DH domains and extending to kilometric (km) wavelengths (covering the entire Sun-Earth distance) are associated with CMEs of the largest energy. This hierarchical relationship implies that all type II bursts as associated with CMEs, i.e., mass ejecta (see Gopalswamy et al., 2005).

If the speed of a CME exceeds the local Alfven speed in the corona and IP medium it can drive a shock, which in turn can accelerate electrons and ions producing a solar energetic particle (SEP) event. The close association between SEP events and fast CMEs implies that SEPs are accelerated by CME-driven shocks (Reames, 1999). About 70 large SEP events were recorded during the SOHO period, most of them occurring around the solar maximum (Gopalswamy et al., 2005). The associated CMEs were fast (average speed ~1500 km/s), wide (mostly full halos) and decelerating (due to coronal drag). Large SEP events with the most energetic particles, ground level enhancements (GLEs), are associated with the fastest CMEs (~2000 km/s). The source regions of the SEP-associated CMEs are generally located on the Sun's western hemisphere, and this distribution is different from that of the CMEs producing geomagnetic storms (Fig. 5). Thus, all frontsided fast and wide CMEs are potentially important for Earth's space weather. An important SOHO result is that the high-intensity SEPs are associated with active regions that produce repeated CMEs, suggesting that CME interactions may be important in accelerating the particles in large SEPs. Emslie et al. (2004) have shown that the CME kinetic energy is the largest component in the energy budget of an eruption. As much as 10% of the CME kinetic energy might go into SEPs, suggesting that CME-driven shocks are very efficient particle accelerators.

4. CMEs in the heliosphere

Signatures of ICMEs

CMEs can carry into the heliosphere large amounts of coronal magnetic fields and plasma, which can be detected by remote sensing and in-situ spacecraft observations. The passage of this material past a single spacecraft is marked by distinctive signatures, but with a great degree of variation from event to event (see Gosling, 1993). These signatures include transient IP shocks, depressed proton temperatures, cosmic ray depressions, flows with enhanced helium abundances, unusual compositions of ions and elements, and magnetic field structures consistent with looplike topologies.

A widely used single-parameter signature of ejecta is the occurrence of counterstreaming suprathermal electrons. Since suprathermal electrons carry electron heat flux away from the Sun along magnetic field lines, when found streaming in both directions along the field they are interpreted as signatures of closed field lines and, thus, as a good proxy for CMEs in the solar wind (see Gosling, 1993). An important multiple signature of an IP (I) CME, is a magnetic cloud, defined as

several-hour flows with large-scale rotations of unusually strong magnetic field accompanied by low ion temperatures. The magnetic field data from clouds often provide good fits to flux rope models.

Another class of ejecta plasma signatures are the abundances and charge state compositions of elements and ions which are systematically different in ICMEs compared with other kinds of solar wind (von Steiger & Zurbuchen, 2003; Richardson and Cane, 2004). As the corona expands outward, the electron density decreases so rapidly that the plasma becomes collisionless and the relative ionization states become constant, thus reflecting the conditions of origin in the corona. The charge states of minor ions in CME flows usually suggest slightly hotter than normal coronal conditions (i.e., >2 MK) at this "freezing in" location. In addition, transient flows often exhibit element and ion abundances that are enhanced relative to the typical solar wind. Unusually low ionization states of He and minor ions have also been detected in CME flows. Although rarely observed before, enhanced He^+ flows have been associated with several recent halo CMEs with more sensitive instruments on the SOHO, Wind and ACE spacecraft. In each of these events an erupting filament-halo CME could be associated with either a dense and compact 'plug' or an extended flow of cool plasma in the trailing edge of a magnetic cloud. This is likely material from the filament itself, consistent with near-Sun observations showing that erupting filaments lag well behind the leading edge of their associated CMEs.

Remote sensing of CMEs

Several techniques have been developed to remotely detect and track disturbances related to CMEs in the IP medium, mostly using radio and white light wavelengths to detect and crudely image these structures. The radio techniques are the km-wavelength radio observations from space and interplanetary scintillation (IPS) observations from the ground. The km-wavelength observations can track the type II emission typically from strong shocks traveling ahead of fast CMEs. Such instruments have been flown on the ISEE-3, Wind and Ulysses spacecraft, and will be on the twin STEREO spacecraft to be launched in 2006. The IPS technique relies on measurements of the fluctuating intensity level of signals from strong, point-like distant radio sources from one or more ground arrays operating in the MHz range. IPS arrays detect changes in density inhomogeneties in the (local) IP medium moving across the line of sight to the source. Disturbances are detected by either an enhancement of the scintillation level and/or an increase in velocity. The technique suffers from relatively poor temporal (~24 hour) and spatial (few bright sources) resolution, ionospheric noise which limits viewing near the Sun and near the horizon, and a model-dependence for interpreting the signal as density or mass.

Heliospheric observations in white light of ICMEs were first made by the zodiacal light photometers on the twin Helios spacecraft, which orbited the Sun in the 1970s and early 1980s. Like solar coronagraphs, Helios detected ICMEs by the Thomson scattering process. The Helios photometers provided the heritage for an instrument called the Solar Mass Ejection Imager (SMEI), developed as a proof-of-concept experiment for operational forecasting (Eyles et al., 2003). Launched in January 2003 on the Coriolis spacecraft, SMEI images nearly the entire sky in white light once per spacecraft orbit, using three baffled camera systems with CCD detectors. Individual frames are mapped into ecliptic coordinates to produce a nearly complete sky map (Fig. 7) every 100 min. During its first 3 years SMEI has observed over 200 CMEs (Webb et al., 2006). SMEI has detected and tracked ~30 Earth-directed ("halo") CMEs. Fig. 7 shows the first, a fast (~1000 km/s) event detected by SMEI 15 hours before it reached Earth and caused a major geomagnetic storm. If it continues operating, SMEI may provide IP context observations for the STEREO mission, which includes limited-field Heliospheric Imagers.

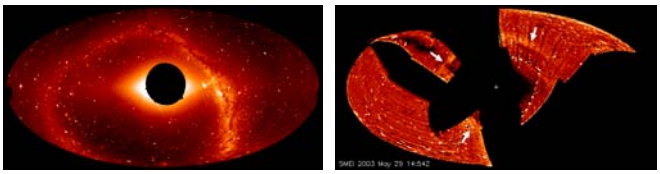

Fig. 7. All-sky images from SMEI. (Left) Composite image in Feb. 2003. Equal-area Hammer-Aitoff projection centered on Sun with North and South ecliptic poles at top and bottom. Dark circle is zone of exclusion 20^o in radius centered on Sun. (Right) Earthward halo CME seen from SMEI on May 29, 2003. The halo was visible as an arc over $>150^o$ of sky (arrows). Black areas are due to shuttering of bright sunlight and CCD noise from particles in Earth orbit.

5. The importance and geoeffectiveness of CMEs

CMEs are responsible for the most geoeffective solar wind disturbances and, therefore, the largest storms. Enhanced solar wind speeds and southward magnetic fields associated with IP shocks and ejecta are known to be important causes of storms (see Tsurutani et al., 1988; Gosling et al., 1991). Since the launch of SOHO, halo CMEs have been used to study the influence of Earth-directed CMEs on geoactivity (Fig. 8). Webb et al. (2000), Cane et al. (2000), St. Cyr et al. (2000), Cane & Richardson (2003) and Zhao & Webb (2003) all found good associations between frontside halo CMEs and ejecta signatures at 1 AU, especially around solar minimum, with varying degrees of correspondence over other parts of the cycle. Webb et al. (2000) found that all 6 frontside halos in early 1997 with surface sources near sun center were associated with magnetic clouds and moderate-level storms at Earth. St. Cyr et al. (2000) found similar, but weaker associations between halo CMEs and storms, concluding that 83% of intense storms were preceded by frontside halo CMEs. However, 25 of the frontside halo CMEs did not produce such large storms and were, therefore,

false alarms.

Full (360º) halo events (Fig. 8) are the most likely to be directed along the Sun-Earth line and those with frontside sources should be Earth-directed. In a study of 89 frontside full halo (FFH) CMEs observed from 1996-2000, Webb (2002) found that ~70% of the halos were associated with shocks and/or other ejecta signatures at 1 AU, and 60% with magnetic cloud-like structures. However, Cane & Richardson (2003), using data from 1996-2002, concluded that only about half of all frontside halo CMEs have associated ejecta at Earth, even if only FFH CMEs are considered. Schwenn et al. (2005) found that 85% of all FFH CMEs become ejecta at Earth.

Zhao & Webb (2003) studied the storm effectiveness of FFH CMEs observed from 1996-2000. The fractional association between the FFH CMEs and moderate or intense storms (peak *Dst* < -50nT) decreased from 0.9 in 1997 to 0.4 in 1999, then increased to 0.7 at maximum in 2000. Thus, on average 65% of the FFH CMEs were associated with moderate-level or greater storms. Gopalswamy et al. (2005) found that most intense storms (*Dst* < -100nT) are caused by fast halo CMEs. Webb (2002) showed that the average travel time of the geoeffective halo CMEs to Earth was 3.3 days, and that the average CME rate and speeds increased with the cycle while the travel time decreased, as expected for more energetic events. Thus, we can conclude that halo CMEs with associated surface features near Sun center usually presage at least moderate geomagnetic storms, but that many such storms occur without halo-CME forewarning. But the simple observation of the occurrence of a frontside halolike CME has increased our ability to forecast the occurrence of moderate or greater storms. Moderate storms without CMEs are usually caused by Earth passage through the heliospheric current sheet (HCS) and related corotating interaction regions (CIRs).

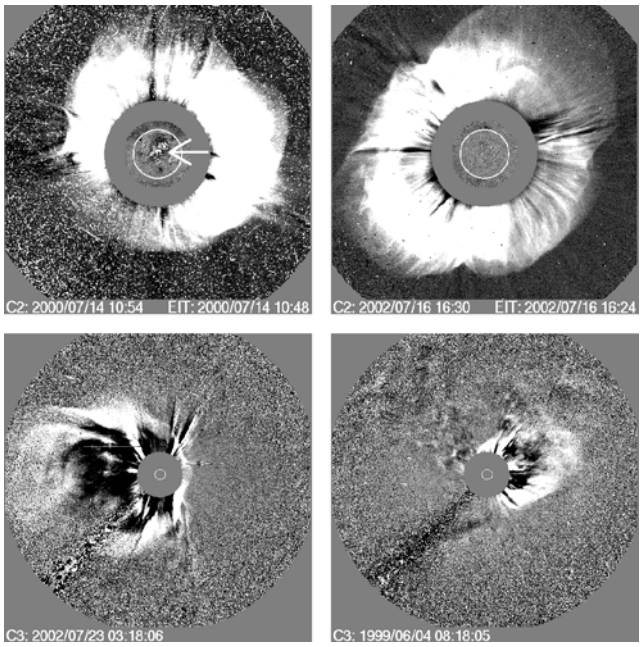

Fig. 8. (Top) Examples of variety of halo CMEs, clockwise: a frontside full halo (source near Sun center), a backside full halo, a partial halo and an asymmetric full halo. From Gopalswamy et al. (2005).

Why are CMEs in general and halo CMEs in particular less well associated with storms near solar maximum than minimum? There are several possible reasons. The occurrence rate of CMEs increases by an order of magnitude near maximum, leading to multiple CMEs per day over the Sun or even from a single region. Gopalswamy et al. (2001) found evidence for interacting CMEs wherein a faster CME overtakes a slower one near the Sun, producing a collision or interaction. Reconnection or sandwiching of each CMEs's field lines are likely in such cases. The combination of sequential eruptions and their subsequent interactions can produce complex ejecta at 1 AU. Such ejecta often consist of high speed flows with shocks and other ICME signatures, but poorly defined magnetic structures, or 'tangled fields' (Burlaga et al., 2001). In addition, the rate at which CMEs actually encounter Earth near maximum is modified by their broadening latitude distribution. Thus, although the CME rate is considerably higher at maximum, proportionally fewer CMEs are ejected near the ecliptic because of the highly tilted streamer belt. Because the flux ropes associated with this tilted belt tend to be north-south oriented, the individual CMEs reaching the ecliptic may contain little southward field. Finally, the "background" solar wind into which the CMEs are injected is itself more complex near maximum, leading to distortions and compressions that are difficult to simulate and predict.

Most SEP events during SOHO were associated with the energetic m-to-km type II bursts. Early observations of m-to-km type II bursts and their associated CMEs can provide advanced warning on SEPs and energetic plasmas

propagating toward Earth or parts of the inner heliosphere and are thus important for future manned exploration.

6. Summary and conclusions

The distribution of geomagnetic disturbances over the solar activity cycle tends to have two peaks representing two major components of geoactivity with different solar and heliospheric sources: one associated with transient solar activity, CMEs, that peaks with the sunspot cycle, and the other associated with recurrent CIRs, CMEs and high speed streams from coronal holes during the declining phase. In terms of space weather, CMEs are the most important transient activity because they link the activity at the Sun and its propagation through the heliosphere to Earth and cause the largest storms. However, both CMEs and CIR-high speed stream ensembles can be geoeffective at all phases of the cycle.

What makes solar and heliospheric disturbances geoeffective, in terms of causing storms, is primarily due to southward IMF and compression. Southward IMF is important because it allows merging of the IMF and Earth's magnetic field and transfer of solar wind energy and mass into the magnetosphere. Compression is important because it strengthens existing southward IMF and, to a lesser extent, increases density. CMEs usually contain long-duration flows of southward IMF and fast CMEs compress any southward field ahead. Sometimes the geoeffective compressed, southward field can be entirely within the shock "sheath". In addition, CMEs themselves can carry high-density structures, such as solar filaments. High-speed streams are geoeffective when they compress any southward IMF in CIRs, and also because they are associated with the acceleration of electrons in the magnetosphere to hazardous levels.

Acknowledgments. We thank the Organizing Committee of the 2006 ILWS Workshop for inviting this presentation. We benefited from data from the SOHO mission, which is an international collaboration between NASA and ESA, and also from the SOHO/LASCO CME catalog, generated and maintained by the Center for Solar Physics and Space Weather, The Catholic University of America in cooperation with NRL and NASA. We thank S. Kahler and E. Cliver for reviewing the manuscript. This work was supported at Boston College by Air Force contract AF19628-00-K-0073 and Navy grant N00173-01-1-G013.

References

S. K. Antiochos, C. R. DeVore and J. A. Klimchuk, *Astrophys. J.*, vol. 510, pp. 485-493, 1999.

D. A. Biesecker, D. C. Myers, B. J. Thompson, D. M. Hammer and A. Vourlidas, *Astrophys. J.*, vol. 569, pp. 1009-1015., 2002.

G. E. Brueckner et al., *Solar Phys.*, vol. 162, pp. 357-402, 1995.

J. T. Burkepile, A. J. Hundhuasen, A. L. Stanger, O. C. St. Cyr and J.A. Seiden, *J. Geophys. Res.*, vol. 109, A03103, doi:10.1029/2003JA010149, 2004.

L. F. Burlaga, R. M. Skoug, C. W. Smith, D. F. Webb, T.H. Zurbuchen and A. Reinard, *J. Geophys. Res.*, vol. 106, p. 20957, 2001.

H. V. Cane and I. G. Richardson, *J. Geophys. Res.*, vol. 108, p. 1156, doi:10.1029/2002JA009817, 2003.

H. V. Cane, I. G. Richardson and O. C. St. Cyr, *Geophys. Res. Lett.*, vol. 27, pp. 3591-3594, 2000.

R. F. Canfield, H. S. Hudson and D. E. McKenzie, *Geophys. Res. Lett.*, vol. 26, p. 627, 1999.

E. W. Cliver and H.S. Hudson, *J. Atmos. Sol. Terr. Phys.*, vol. 64, pp. 231-252, 2002.

E. W. Cliver, D. F. Webb and R. A. Howard, *Solar Phys.*, vol. 187, p. 89, 1999.

E. W. Cliver, M. Laurenza, M. Storini and B. J. Thompson, *Astrophys. J.*, vol. 631, pp. 604-611, 2005.

A. G. Emslie et al., *J. Geophys. Res.*, vol. 109, A10104, doi :10.1029/2004JA010571, 2004.

C. J. Eyles et al., *Solar Phys.*, vol. 217, pp. 319-347, 2003.

N. Gopalswamy, in *The Sun and the Heliosphere as an Integrated System*, ASSL, G. Poletto and S. Suess, Eds. Kluwer, Boston, 2004, pp. 201-252.

N. Gopalswamy, J. *Astrophys. Astron.*, vol. 27, pp. 243-254, 2006.

N. Gopalswamy and M.R. Kundu, *Solar Phys.*, vol. 143, p. 327, 1993.

N. Gopalswamy, S. Yashiro, M.L. Kaiser, R.A. Howard and J. -L. Bougeret, *Astrophys. J.*, vol. 548, pp. L91-L94, 2001.

N. Gopalswamy, M. Shimojo, W. Lu, S. Yashiro, K. Shibasaki and R.A. Howard, *Astophys. J.*, vol. 586, p. 562, 2003.

N. Gopalswamy, B. Fleck and J. B. Gurman, in *Proc. of Asia Pacific Regional Conf. of IAA "Bringing Space Benefits to the Asia Region"*, R. Mukund and R. Murthy, Eds. in press, 2005.

J. T. Gosling, *J. Geophys. Res.*, vol. 98, pp. 18937-18949, 1993.

J. T. Gosling, D. J. McComas, J. L. Phillips and S. J. Bame, *J. Geophys. Res.*, vol. 96, pp. 7831-7839, 1991.

R. A. Harrison, *Astron. Astrophys.*, vol. 162, pp. 283-291, 1986.

R. A. Howard, D. J. Michels, N. R. Sheeley, Jr. and M. J. Koomen, *Astrophys. J.*, vol. 263, pp. L101-L104, 1982.

R. A. Howard, N. R. Sheeley Jr., M. J. Koomen and D. J. Michels, *J. Geophys. Res.*, vol. 90, pp. 8173-8191, 1985.

R. A. Howard, N. R. Sheeley Jr., D. J. Michels and M. J. Koomen, in *The Sun and Heliosphere in Three Dimensions*, R. G. Marsden, Ed. D. Reidel, Dordrecht, Holland, 1986, pp. 107-111.

R. A., Howard, J. Morrill, A. Vourlidas, D. Buzasi, E. Esfandiari, N. Rich and A. Thernisien, *Fall 2003 AGU meeting abstracts*, F1222, 2003.

H. S. Hudson, *Solar Phys.*, vol. 133, p. 357 1991.

H. S. Hudson and E. W. Cliver, *J. Geophys. Res.*, vol. 106, pp. 25199-25213, 2001.

H. S. Hudson and D. F. Webb, in *Coronal Mass Ejections*, N. Crooker et al, Eds. GM 99, Washington, D.C., AGU, 1997, p. 27.

A. J. Hundhausen, *J. Geophys. Res.*, vol. 98, pp. 13177-13200, 1993.

A. J. Hundhausen, J. T. Burkepile and O. C. St. Cyr, *J. Geophys. Res.* vol. 99, pp. 6543-6552, 1994.

S. W. Kahler, *Astrophys. J.*, vol. 214, pp. 891-897, 1977.

S. W. Kahler, *Annu. Rev. Astron. Astrophys.*, vol. 30, p. 113, 1992.

S. W. Kahler, in *Chapman Conference on Solar Energetic Plasmas and Particles*, N. Gopalswamy and J. Torsti, Eds. AGU GM, Washington, DC, in press, 2006.

P. H. Munro et al., *Solar Phys.*, vol. 61, p. 201, 1979.

N. Nitta and S. Akiyama, *Astrophys. J.*, vol. 525, p. L57, 1999.

S. P. Plunkett et al., *Adv. Space Res.*, vol. 29, pp. 1473-1488, 2002.

R. Ramesh, C. Kathiravan and C. V. Sastry, *Astrophys. J.*, vol. 591, p. L163, 2003.

D. V. Reames, *Space Sci. Rev.*, vol. 90, p. 413, 1999.

I. G. Richardson and H. V. Cane, *J. Geophys. Res.*, vol. 109, A09104, doi:10.1029/2004JA010598, 2004.

I. G. Richardson, H. V. Cane and E. W. Cliver, *J. Geophys. Res.*, vol. 107, doi: 10.1029/2001JA000504, 2002.

D. M. Rust and E. Hildner, *Solar Phys.*, vol. 48, p. 381, 1976.

D. M. Rust and D. F. Webb, *Solar Phys.*, vol. 54, p. 403, 1977.

R. Schwenn, A. Dal Lago, E. Huttunen and W. D. Gonzalez, *Ann. Geophys.*, vol. 23, p. 1033, 2005.

N. R. Sheeley, Jr., R. A. Howard, M. J. Koomen and D. M. Michels, *Astrophys. J.*, vol. 272, pp. 349-354, 1983.

A. C. Sterling, H. S. Hudson, B. J. Thompson and D. M. Zarro, *Astrophys. J.*, vol. 532, pp. 628-647, 2000.

O. C. St. Cyr et al., *J. Geophys. Res.*, vol. 105, pp. 18169-18185, 2000.

B. J. Thompson, E. W. Cliver, N. Nitta, C. Delannee and J. P. Delaboudiniere, *Geophys. Res. Lett.*, vol. 27, pp. 1431-1434, 2000.

D. Tripathi, V. Bothmer and H. Cremades, *Astron. Astrophys.* vol. 422, pp. 337-349, 2004.

B. T. Tsurutani, W. D. Gonzalez, F. Tang, S. I. Akasofu and E. J. Smith, *J. Geophys. Res.*, vol. 93, pp. 8519-8531, 1988.

R. Von Steiger and T. H. Zurbuchen, in *Solar Variability as an Input to the Earth's Environment*, ESA SP-535, A. Wilson, Ed. ESTEC, Noordwijk, The Netherlands, 2003, pp. 835-840.

A. Vourlidas, K. P. Subramanian, K. P. Dere and R. A. Howard, *Astrophys. J.*, vol. 534, pp. 456-467, 2000.

A. Vourlidas, D. Buzasi, R. A. Howard and E. Esfandiari, in *Solar Variability: From Core to Outer Frontiers*, ESA SP-506, A. Wilson, Ed. ESTEC, Noordwijk, Netherlands, 2002, pp. 91-94.

D. F. Webb, in *From Solar Min to Max: Half a Solar Cycle with SOHO*, ESA SP-508, A. Wilson, Ed. ESTEC, Noordwijk, Netherlands, 2002, p. 409.

D. F. Webb and R. A. Howard, *J. Geophys. Res.*, vol. 99, p. 4201, 1994.

D. F. Webb, R. A. Howard and B. V. Jackson, in *Solar Wind Eight*, D. Winterhalter et al., Eds. AIP Conf. Proc. 382. Woodbury, N.Y., 1996, pp. 540-543.

D. Webb, S. Kahler, P. McIntosh and J. Klimchuk, *J. Geophys. Res.*, vol. 102, pp. 24161-24174, 1997.

D. F. Webb, E. W. Cliver, N. U. Crooker, O. C. St. Cyr and B. J. Thompson, *J. Geophys. Res.*, vol. 105, pp. 7491-7508, 2000.

D. F. Webb et al., *J. Geophys. Res.*, in press, 2006.

S. Yashiro et al., *J. Geophys. Res.*, vol. 109, A07105, doi:10.1029/2003JA010282, 2004.

X. P. Zhao and D. F. Webb, *J. Geophys. Res.*, vol. 108, p. 1234, doi:10.1029/2002JA009606, 2003.